The FANCC-FANCE-FANCF complex is evolutionarily conserved and regulates meiotic recombination

Dipesh Kumar Singh[1], Rigel Salinas Gamboa[1], Avinash Kumar Singh[2], Birgit Walkemeir[1], Jelle Van Leene[3,3bis], Geert De Jaeger[3,3bis], Imran Siddiqi[2], Raphael Guerois[4], Wayne Crismani[5,6] and Raphael Mercier[1*]

[1]Department of Chromosome Biology, Max Planck Institute for Plant Breeding Research, Carl-von-Linné-Weg 10, 50829 Cologne, Germany

[2] CSIR-Centre for Cellular & Molecular Biology, Uppal Road, Hyderabad, 500007, India

[3] Department of Plant Biotechnology and Bioinformatics, Ghent University, Ghent, B-9052, Belgium

[3bis] Center for Plant Systems Biology, VIB, Ghent, B-9052, Belgium

[4] Institute for Integrative Biology of the Cell (I2BC), Commissariat à l'Energie Atomique, CNRS, Université Paris-Sud, Université Paris-Saclay, Gif-sur-Yvette, 91190, France

[5] The DNA Repair and Recombination Laboratory, St Vincent's Institute of Medical Research, Melbourne, 3065, Australia,

[6] The Faculty of Medicine, Dentistry and Health Science, The University of Melbourne, Parkville, Victoria, Australia

*Corresponding author: Raphael Mercier (mercier@mpipz.mpg.de)

Abstract

At meiosis, programmed meiotic DNA double-strand breaks are repaired *via* homologous recombination, resulting in crossovers (COs). From a large excess of DNA double-strand breaks that are formed, only a small proportion gets converted into COs because of active mechanisms that restrict CO formation. The Fanconi anemia (FA) complex proteins AtFANCM, MHF1, and MHF2 were previously identified in a genetic screen as anti-CO factors that function during meiosis in *Arabidopsis thaliana*. Here, pursuing the same screen, we identify FANCC as a new anti-CO gene. FANCC was previously only identified in mammals because of low primary sequence conservation. We show that FANCC, and its physical interaction with FANCE-FANCF, is conserved from vertebrates to plants. Further, we show that FANCC, together with its subcomplex partners FANCE and FANCF, regulates meiotic recombination. Mutations of any of these three genes partially rescues CO-defective mutants, which is particularly marked in female meiosis. Functional loss of FANCC, FANCE, or FANCF results in synthetic meiotic catastrophe with the pro-CO factor MUS81. This work reveals that FANCC is conserved outside mammals and has an anti-CO role during meiosis together with FANCE and FANCF.

Introduction

Large-scale exchange of genetic material between homologous chromosomes in the form of meiotic crossovers (COs) generates new allelic combinations in the sexual progeny of eukaryotes. COs are also required for the correct segregation of chromosomes at the first meiotic division in most species. This is likely why a mechanism exists to ensure an “obligate” crossover per chromosome pair, per meiosis. Meiotic recombination is initiated by the formation of a large number of programmed DNA double-stranded breaks (DSBs), a minority of which are repaired as COs. Two

pathways contribute to CO formation, defining two classes of COs. Class I COs depend on a group of proteins called ZMMs, an acronym derived from seven proteins initially described in *Saccharomyces cerevisiae* (Zip1-Zip4, Msh4-5, Mer3) (Pyatnitskaya, Borde, and De Muyt 2019; Borner, Kleckner, and Hunter 2004), and account for most of the COs. Class II COs, which account for a minority of COs in most eukaryotes including mammals and plants, involve notably the MUS81 nuclease (Youds and Boulton 2011; de los Santos et al. 2003).

In *Arabidopsis thaliana*, a mutation in any member of the *ZMMs* causes a drastic decrease in CO number, and notably the loss of the obligate crossover, with only a few residual COs formed by the class II pathway, leading to chromosome mis-segregation and quasi-sterility. A forward genetic screen for restoration of fertility of *zmm* mutants identified a series of genes that actively limit CO formation in Arabidopsis. These factors specifically limit class II COs and act through three mechanisms. The first anti-CO pathway involves proteins from the Fanconi anaemia (FA) pathway, FANCM (Crismani et al. 2012), MHF1, and MHF2 (Girard et al. 2014). These three proteins have been shown to physically interact in humans, along with FAAP24, which has not been identified in Arabidopsis (Singh et al. 2010; Tao et al. 2012). The second anti-CO mechanism involves RECQ4, RMI1, and TOP3a (Seguela-Arnaud et al. 2017), and the third, the proteins FIGL1 and FLIP (Girard et al. 2015; Fernandes, Duhamel, et al. 2018; Kumar et al. 2019). These three mechanisms contribute in parallel to limiting class II COs (Fernandes, Seguela-Arnaud, et al. 2018).

The FA pathway is comprised of at least 23 protein subunits in human cells and some, but not all, of them are widely conserved in eukaryotes, including plants. It is traditionally known for its role in inter-strand crosslink repair in somatic cells in humans, with emerging roles in replication fork protection (Kolinjivadi, Crismani, and Ngeow

2020). The FA pathway is heavily studied because its proper function is required to prevent serious human disease: FA functions as a tumor suppressor and mutation of FA pathway factors causes the rare condition Fanconi anemia. FA core complex proteins have been classified into three groups on the basis of their molecular roles: (i) The core complex encompasses the largest group of proteins and is installed at DNA damage sites or stalled replication forks, with FANCM acting as an anchor. MHF1-MHF2, a heterodimeric protein complex, promotes FANCM recruitment at the site of DNA damage (Yan et al. 2010; Singh et al. 2010). (ii) The FA-ID2 complex is recruited and monoubiquitinated by the core complex at the DNA damage site (Smogorzewska et al. 2007), while it antagonizes the recruitment of FA proteins to chromatin in the absence of DNA damage (Lopez-Martinez et al. 2019). (iii) FA/HR complex proteins are downstream partners that are considered to function independently of the above two groups (Kottemann and Smogorzewska 2013; Deakyne and Mazin 2011).

Structural studies (Shakeel et al. 2019; Swuec et al. 2017; Huang et al. 2014) have demonstrated that seven subunits of the core complex (FANCA, FANCB, FANCC, FANCE, FANCF, FANCG, FANCL), and two FA-associated proteins (FAAP20 and FAAP100) form three different subcomplexes: (i) FANCB-FANCL-FAAP100 (BL100), (ii) FANCC-FANCE-FANCF (CEF), and (iii) FANCA-FANCG-FAAP20 (AG20)(Huang et al. 2014; Rajendra et al. 2014). The ring finger domain of FANCL acts as an E3 ubiquitin ligase and its two associated proteins FANCB and FAAP100 are organized as a catalytic module (Huang et al. 2014; Shakeel et al. 2019). It has been proposed that FANCA and FANCG form a chromatin-targeting module, while FANCC, FANCE, and FANCF organize to establish a substrate-recognition module (Shakeel et al. 2019). FANCF acts as a bridge between FANCC and FANCE (Leveille et al. 2004; Shakeel et al. 2019). FANCM interacts with the core complex through

FANCF (Deans and West 2009; Huang et al. 2014), demonstrating that the substrate-recognition module is an important component of the FA core complex.

In this study, extending a previously described forward genetic *zmm* suppressor screen (Crismani et al. 2012; Girard et al. 2014; Fernandes, Duhamel, et al. 2018; Seguela-Arnaud et al. 2017; Girard et al. 2015), augmented by complementary approaches, we demonstrate that the CEF complex is evolutionarily conserved from mammals and show that it is a novel meiotic anti-CO factor.

Results

Identification of a novel *zmm* suppressor

CO-deficient *zmm* mutants display a > 90% reduced seed set in Arabidopsis, which correlates with shorter fruit, due to random segregation of chromosomes in meiosis. Therefore, inactivating anti-CO genes in a *zmm* mutant leads to an increase in CO number, resulting in improved chromosome segregation, restored fertility and longer fruits. Here, we extended a forward genetic screen for *zmm* mutants exhibiting increase in fruit length following EMS mutagenesis. The screen was previously performed on five *zmm* mutants (*hei10, zip4, shoc1, msh5* and *msh4*), in a total of ~7,000 lines and identified 59 mutants with restored fertility, among which 58 are mutated in one of the previously identified anti-CO genes (Table 1, Table S1). (Girard et al. 2014; Girard et al. 2015; Crismani et al. 2012; Fernandes, Duhamel, et al. 2018; Seguela-Arnaud et al. 2017). In this study, we focused on the last *zmm* suppressor mutation that increased the fertility of a *msh4* mutant (cshl_GT14269, L*er* genetic background). Genetic mapping delimited the causal mutation to a 0.47MB region on chromosome 3 (21452882-21919909 in the Ler assembly)(Zapata et al. 2016), and whole genome sequencing identified a candidate mutation in the fourth exon donor splicing site of the At3g60310 gene (G>A 3_21918909 in the Ler assembly, corresponding to

3_22288z888 in Col TAIR10). We show below that At3g60310 encodes the Arabidopsis FANCC ortholog. Three independent T-DNA alleles (*fancc-2 N542341*, *fancc-3 N1007952* and *fancc-4 N626745*, Col background) were able to enhance the fertility of *msh4*, from 4.5 to >24 seeds per fruit (Figure 1 and Supplementary Figure S1, S2), confirming the identification of the causal mutation in At3g60310.

FANCC is conserved in plants

Standard sequence similarity analysis failed to find any homology of the protein encoded by At3g60310 outside of plants, or with proteins of known function (Stanley et al. 2016). Using the HHpred remote homology detection server (Zimmermann et al. 2018). (Soding 2005), it was possible to identify a potential match with human FANCC (XP_011516668) despite both proteins sharing only 16% primary sequence identity (HHpred probability of 94%). To test the hypothesis that At3g60310 is an ortholog of FANCC, we analyzed the physical contacts between human FANCC and the human FANC complex, the cryo-EM structure of which was recently determined at 3.1 Å (Wang et al. 2021). Figure 2A illustrates that human FANCC (pale green subunit) is in direct physical contact with three subunits of human FA core complex, FANCE (light pink), FANCF (light blue) together with the ubiquitin E3 ligase FANCL (yellow). Given that FANCC, FANCE, and FANCF are known to constitute a stable sub-complex in humans, we tested the possibility that At3g60310 was a dedicated partner of *A. thaliana* FANCE (Girard et al. 2014) (Q9SU89_ARATH) and FANCF (F4K7F0_ARATH) using the Alphafold2 prediction method (Jumper et al. 2021). Alphafold2 was recently shown to perform well when predicting structures of proteins and whether two proteins interact with each other (Evans et al. 2021). Using the AlphaFold2 method trained on multimers (Mirdita, Ovchinnikov, and Steinegger 2021), we obtained a model of the complex with the three *A. thaliana* subunits with reliability

scores above the confidence threshold of 50 and 0.5 for pLDDT and ptmscore, respectively (pLDDT of 72.6 and ptmscore of 0.67) (Supp. Figure S3). Interestingly, At3g60310 was predicted to form a complex with AtFANCE and AtFANCF with a similar arrangement to that observed for the corresponding orthologs in the human FANC complex (Figure 2B). As a support for the reliability of the model, the surface patches of At3g60310 involved in the interaction with both subunits were among the most conserved regions (Figure 2C, Supp Figure S4,S5). The N-terminal domain of FANCE is found well anchored in the central region of At3g60310/FANCC with low predicted error for the accuracy of the interface modelling (Supp Figure S3). In contrast, the C-terminal domain does not exhibit a strong co-evolutionary signal in the region where it binds to At3g60310/FANCC. The five models generated for FANCE do not converge on a single conformation for the C-terminal domain, although due to the tethering of the N-terminal domain, this domain tends to cluster in the same region as the surface where the FANCL E3 Ub ligase binds to FANCC. One hypothesis could be that upon binding of the E3 ligase FANCL, the C-terminal domain of FANCE is displaced from the position shown in Figure 2B to allow FANCL binding, which is potentially coupled with the recruitment of FANCD2 substrate by the FANCE C-terminal domain (Polito et al. 2014).

Next, we performed an unbiased search for interacting partners of At3g60310 using pull-down protein purification coupled with mass spectrometry. We used overexpressed GSrhino-tagged At3g60310 as a bait in Arabidopsis suspension cell culture (Van Leene et al. 2019). After filtering copurified proteins for false positives, we recovered peptides from At3g60310 itself and a series of additional proteins in three replicate experiments (Table 2). Strikingly, all four co-purified identified proteins were Arabidopsis homologs of members of the FA complex, FANCE, FANCL, FANCM, and

MHF2 (Table 2). Further, a yeast two-hybrid assay confirmed direct interactions of At3g60310 with FANCE and MHF2. FANCE, FANCF and MHF2 also interacted with each other in yeast two-hybrid (Figure S6). Altogether, this demonstrates that At3g60310 encodes the FANCC protein in Arabidopsis, which we term AtFANCC.

FANCC is conserved in distant eukaryotic lineages

Using PSI-BLAST searches, AtFANCC orthologs could be detected in most plants (Figures S4 and S5). In-depth analyses using either PSI-BLAST or HHpred failed to detect any homolog in more distantly related green algae such as *Chlamydomonas*, although a FANCE homolog can be detected in *Chlamydomonas reinhardtii*. In metazoans, a previous bioinformatics analysis performed on model species for all the genes of the FANC core complex, noted that several species were missing a FANCC homolog although having a FANCE ortholog (Stanley et al. 2016). We revisited this study using the most recent sequence databases and PSI-BLAST searches starting from human FANCC. Interestingly, five iterations of PSI-BLAST were required to retrieve the first plant ortholog (in the monocot *Spirodela intermedia*), which enabled the retrieval of all the same plant orthologs identified from AtFANCC. After 15 iterations, the search nearly converged with about 2,100 FANCC homologs, highlighting the existence of FANCCs in early branching metazoans such as *Nematostella vectensis* (XP_032241565) and *Ciona intestinalis* (XP_002129616) that were not found previously. In insects, orthologs could also be detected in Hymenoptera (ants and bees) but neither in Diptera (Drosophila) nor in Lepidoptera (Bombyx). Consistently, repeating the PSI-BLAST search with human FANCE or FANCF as queries, a similar distribution of homologs was found in insects. Homologs of FANCE and FANCC could be detected in specific fungal lineages such as *Rhizopus azygosporus* (corresponding to hypothetical proteins RCH90546.1 and RCH79564.1,

respectively). A reciprocal HHpred analysis comparing these genes against the human database confirmed they were remote homologs of FANCE and FANCC (HHpred probability score of 100% and sequence identities of 21% and 15%, respectively), suggesting that certain fungal lineages did not lose these FANC complex subunits.

Atfancc, Atfance, and *Atfancf* mutations increase fertility and bivalent formation of crossover-deficient *zmm* mutants.

As the mammalian FANCC was shown to form a structural and functional module with FANCE and FANCF ((Shakeel et al. 2019; Swuec et al. 2017; Wang et al. 2021), we explored their potential meiotic roles in parallel. A FANCE homolog was previously described in Arabidopsis (Girard et al. 2014), and the AT5G44010 gene was annotated as *AtFANCF* in Araport11 because of sequence similarity with the mammalian *FANCF* (Cheng et al. 2017). Single mutants in each of these genes did not show growth or developmental defects but had a slight decrease in fertility (Figure 1, Figure S2). Meiotic chromosome spreads in *Atfance* and *Atfancf* single mutants revealed the presence of univalents at low frequencies, showing that some chromosome pairs lack COs (Figure S7, Figure 3). Combination of *fancc, fance* and *fancf* mutations did not reveal any developmental defects or enhanced sterility and meiotic defects (Figures 1,3). This suggests that, consistent with the pull-down and Y2H data, FANCC, FANCE, and FANCF act together at meiosis, playing a role in ensuring the obligate CO.

Mutation of *FANCC*, or *FANCE*, or *FANCF* significantly restored the fertility of the *zmm* mutants *msh4* and *msh5*, increasing the seed set more than fourfold (Sidak test, $p<10^{-6}$) (Figure1, Figure S2). In the Ler background, chromosome spreads of male meiosis showed an increase of bivalent frequency in *fancc-1 msh4* compared to *msh4* ($p<0.001$) (Figure 3). In comparable experiments in the Col background, *fancc*, *fance*, or *fancf* individual mutations barely increased bivalents in *msh4* (p=0.12, 0.12 and

0.0002, respectively) (Figure 3). Combining Col *fance, fance,* and *fancf* mutations in *msh4* further restored bivalent formation to reach an average of 2.8 bivalents/cell compared to 1.4 in *msh4* ($p<0.0001$) and led to a slightly higher fertility increase compared to *fancc msh4* ($p=0.04$). Altogether, this suggests that FANCC, FANCE, and FANCF limit CO formation in a partially redundant manner. Note that this restoration of bivalent formation is lesser than that obtained through mutation of *FANCM* (5 bivalents; (Crismani et al. 2012)), MHF1 or MHF2 (3.6; Figure 3G, (Girard et al. 2014)), suggesting that the FANCC-FANCE-FANCF module has a supporting role in limiting a portion of the COs prevented by FANCM-MHF1-MHF2. The *fancc* mutation did not further restore bivalent formation in *mhf1 msh4* (t-test $p=0.56$), suggesting that FANCC acts in the same anti-CO pathway as MHF1 (Figure 3G).

FANCC, FANCE, and FANCF regulate meiotic crossover formation

Intriguingly, in the above experiments, we found that *fancc*, *fance,* and *fancf* increased the fertility of *zmm* mutants (*msh4 and msh5*), but that the increase of bivalent number in male meiotic cells was less robust than the seed set suggested. As fertility in the self-pollinating plant Arabidopsis depends on both male and female meiosis, this may suggest that the role of FANCC, FANCE, and FANCF in limiting COs is more critical in female meiosis than in male meiosis. To check this, we used a test line for recombination (FTL420), which contains two transgenes conferring expression of GFP and RFP in the seed coat and defining a 5-Mb interval of the sub-telomeric region on chromosome 3 (Ziolkowski et al. 2015; Melamed-Bessudo et al. 2005). Crossover frequency was measured for males and females separately, through reciprocal crosses with wild-type plants, and in selfing (figure 4, table S 2). In females, recombination was significantly increased (Fisher test, $p<0.0001$) in *fancc* and *fancc fance fancf* compared

to wild type, confirming the anti-CO function of *FANCC.* In males, crossover frequency was not increased, but slightly reduced (p=0.17 for fancc and 0.015 for *fancc fance fancf*). In selfing, which combines male and female meiosis products, recombination was modestly increased in *fancc* compared to wild type (p=0.003). A similar recombination picture was observed in *fance*, *fancf*, and the triple mutant *fancc fance fancf*, suggesting that the three proteins act together in limiting meiotic crossovers.

Atfancc, _Atfance_, and _Atfancf_ exhibit chromosome fragmentation in the _mus81_ background.

Because of the roles of FANCM, MHF1, and MHF2 in preventing class II COs, combining mutation in these genes with mutation of *MUS81* that catalyses class II COs, leads to chromosome fragmentation at meiosis, resulting in sterility. In addition, the *fancm mus81* double mutant shows a strong developmental defect, demonstrating the role of these two genes in somatic DNA repair (Girard et al. 2014; Crismani et al. 2012) When we combined *fancc*, *fance*, or *fancf* with the *mus81* mutation, we did not observe developmental defects. However, in double mutants with *mus81* and either *fanc-c*, *-e*, or *-f* we observed a strong reduction in fertility, measured by seed per fruit, compared to the respective single mutants (Figure 5A, S8). Meiotic chromosome spreads revealed the presence of chromosome fragments at anaphase I and subsequent stages in ~40% of the cells of the double mutants (Figures 5 B–J, S9 A–D and F–J). This demonstrates that FANCC, FANCE, and FANCF are important for efficient DSB repair in a *mus81* background and suggests that they regulate class II CO formation but with a less critical role than FANCM and MHF1/2. The removal of all four genes – *mus81 fancc fance fancf* – did not drastically enhanced fertility defects or chromosome fragmentation compared to the double *mus81 fanc* combinations. These results

277 support the hypothesis that all three genes, *FANCC, FANCE*, and *FANCF*, are required
278 at meiosis to repair a subset of intermediates that can also be repaired by MUS81.
279

280 **Discussion**

281 FANCC-FANCE-FANCF constitute a stable sub-complex within the FA core complex.
282 Based on sequence conservation, FANCE and FANCF homologs have been identified
283 in evolutionarily distant eukaryotes such as plants (Girard et al. 2014; Cheng et al.
284 2017). However, despite multiple studies that systematically catalogued FA pathway
285 protein conservation across diverse taxa, homologs of FANCC have not been identified
286 beyond vertebrates (Zhang et al. 2009; Girard et al. 2014), suggesting that FANCC
287 may not be conserved over large evolutionary scales. Here, combining genetics, *in*
288 *vivo* pull-downs, direct protein-protein interaction studies, and structural modeling, we
289 unambiguously identified the FANCC protein in Arabidopsis. In addition, interaction
290 and modeling studies strongly suggest that FANCC, FANCE, and FANCF form a sub-
291 complex in Arabidopsis as they do in vertebrates. Homologs of FANCC can also be
292 readily identified in most other plants. As the plant and animal branches diverged very
293 early in the eukaryotic tree of life (Burki et al. 2020), this suggests that the FA complex
294 and notably the FANCC-E-F subcomplex was already present in the common ancestor
295 of all living eukaryotes. The algorithm we used to detect divergent homologs
296 succeeded in detecting the link between plant and vertebrate FANCC but failed to
297 detect homologs in fungal lineages, except for a few species. As fungi are more closely
298 related to animals than plants, this suggests that most of the fungal lineages have lost
299 FANCC, or that the FANCC sequence has diverged beyond what we can recognize
300 with current tools. Similarly, FANCC was detected in diverse animal lineages including

some insects, but not in Drosophila, which can be attributed either to gene loss or to extreme divergence.

We initially identified *FANCC* because its mutation can partially restore the fertility of CO-defective *zmm* mutants, in a similar manner to previously identified anti-CO factors and notably the FA complex components FANCM, MHF1, and MHF2 (Crismani et al. 2012; Girard et al. 2014). We also found that mutation in either of the two other subunits of the FA CEF subcomplex, *fance* and *fancf*, improves the fertility of *zmm* mutants. Mutations in the three genes individually restored fertility of *zmm* to similar levels, but to a much lower level than previously obtained with *mhf1*, *mhf2* or *fancm*. Further, restoration of *zmm* fertility upon cumulative mutations in *fancc, fance,* and *fancf* remained limited. This suggests that FANCC, FANCE and FANCF together regulate meiotic recombination, but with a less critical role than FANCM, MHF1, and MHF2. We observed an increased number of bivalents at male meiosis when mutating *fancc*, *fance*, and *fancf* in *zmm* mutants, consistent with an anti-CO function. However, the increase in bivalents in males was limited compared to the observed increase in fertility, suggesting that male and female meiosis could be differently affected. We also observed a slight decrease in fertility and a low frequency of univalents in male meiocytes in single *fancc*, *fance*, or *fancf* mutants, suggesting a pro-CO function. Technical limitations prevented us from measuring the frequency of bivalents/univalents in female meiosis. However, when assessing recombination by a genetic assay in *fancc* and *fancc fance fancf*, we observed a large increase in recombination in females and a small decrease in males. Altogether, we propose that FANCC-E-F regulates meiotic recombination, with a predominant anti-CO function in females, explaining the capacity of their mutation to restore the fertility of *zmm* mutants.

Similar to FANCM and MHF1/MH2, we propose that FANCC-E-F prevents the formation of class II COs that are catalyzed by MUS81. Indeed, combining any of *fancc*, *fance* or *fancf* with the *mus81* mutation led to chromosome fragmentation at meiosis and reduced fertility (Figure 5). Combining the three mutations (*fancc fance fancf*) together had only a slightly increased effect compared to single mutants in the capacity to increase fertility and bivalents of *zmm* mutants (Figure 1 and 3) or for synthetic meiotic catastrophe and reduced fertility when combined with *mus81* (Figure 5). Further, the recombination assay did not detect differences between the single *fancc* and the triple *fancc fance fancf* (Figure 4), suggesting that FANCC-FANCE-FANCF act together in regulating recombination. In all experiments, the observed effects – even when combining the three *fancc fance fancf* mutations – are weaker than observed with MHF1/2 or FANCM (Crismani et al. 2012; Girard et al. 2014). Further, the *fancc-2* has no additive effect with *mhf1* (figure 3). Altogether, this shows that FANCC-FANCE-FANCF acts in the same anti-CO pathway as FANCM-MHF1/2, as also supported by the fact that they form a stable complex *in vivo* (Table1). We propose that FANCC-FANCE-FANCF supports FANCM activity, which unwinds recombination intermediates and directs them to non-crossover repair. We favor the hypothesis that the meiotic crossover-limiting role of Arabidopsis FANCC-E-F is distinct from the well-described somatic role of human FANC-C-E-F where it facilitates FANCD2-FANCI mono-ubiquitination in inter-strand crosslink repair. This hypothesis is supported by the following lines of evidence: 1) There is no detectable crossover-limiting role of neither of the Arabidopsis orthologues of the catalytic component of the human FA core complex – the E3 RING ligase, FANCL – and its substrate FANCD2-FANCI (Girard et al. 2014; Kurzbauer et al. 2018); 2) Human FANCM has well-described functions distinct from the FA core complex (Walden and Deans 2014; Deans and West 2009; Ito and Nishino 2021) that are associated with remodeling branched DNA structures.

351 The FANCC-E-F complex may act to stabilize or support the activity of FANCM in
352 performing its function of branched molecule dissolution during meiotic DSB repair.

Materials and methods

Genetic material: The following Arabidopsis lines were used in this study: *fancc-2* (N542341), *fancc-3*(N1007952), *fancc-4* (N626745), *fance* (N553587) (Girard et al. 2014) *fancf* (N457070) msh4 (N636296(Higgins et al. 2008), *msh5-2* (N526553)(Higgins et al. 2008), *mus81*-2 (N607515) (Berchowitz et al. 2007), and *mhf1-3*(N576310) (Girard et al. 2014). All the T-DNA mutants were obtained from the NASC.

Genetic analysis

The msh4 suppressor *Atfancc* was sequenced using Illumina technology at The Genome Analysis Centre, Norwich, UK, and mutations were identified using ler 1 assembly as reported for the MutDetect pipeline (Girard et al. 2014; Schneeberger et al. 2011). The identified causal mutation in fancc-1 was a G to A substitution at position chr3: 21918909 (Ler-0 TAIR10 assembly) equivalent to position chr3: 22288888 in the Columbia (TAIR10) genome. The primers used for genotyping are listed in Table S3. Siliques were fixed in 70% ethanol for at least two days and scanned for seed counting manually on images. Fertility was assessed by counting seeds per fruit on a minimum of five plants and ten fruits from each plant.

Sequence analyses

Sequences of *A. thaliana* At3g60310/AtFANCC, FANCE (Q9SU89_ARATH) and FANCF (F4K7F0_ARATH) were used as input for the HHpred remote homology detection server against different eukaryotic profile databases (Zimmermann et al. 2018)(Soding 2005) and as queries of PSI-BLAST searches (Altschul et al. 1997) against the nr database. Full-length sequences of FANCC orthologs were retrieved and re-aligned with mafft (Katoh and Standley 2013) and the multiple sequence

379 alignment was represented using JalView (Waterhouse et al. 2009). The phylogenetic
380 tree of the FANCC orthologs in plants was generated using the FANCC MSA as a
381 query of the PhyML 3.0 server (Dereeper et al. 2008) with standard estimated options,
382 an approximate likelihood-ratio test to estimate the bootstrap values (SH-like), and the
383 Jones-Taylor-Thornton substitution model with four substitution rate categories. The
384 calculated tree was represented using the iTOL server (Letunic and Bork 2021).
385
386 Structural modeling
387 Sequences of *A. thaliana* At3g60310/AtFANCC, FANCE (Q9SU89_ARATH) and
388 FANCF (F4K7F0_ARATH, the) query sequences of each subunits were used as input
389 for the MMseqs2 homology search program (Steinegger and Soding 2017) to generate
390 a multiple sequence alignment (MSA) against the UniRef30 clustered database for
391 each of the FANC complex subunits (Mirdita et al. 2017). The calculated full-length
392 sequences of the orthologs were retrieved and re-aligned with mafft (Katoh and
393 Standley 2013). MSAs of FANCC, FANCE and FANCF were then concatenated,
394 matching the sequences of the same species resulting in paired alignments, which
395 were combined with the unpaired sequences for those species that could have not
396 have been matched. The resulting paired plus unpaired concatenated MSA was used
397 as input to generate five structural models of the FANCC-FANCE-FANCF complex
398 using a local version of the ColabFold interface (Mirdita, Ovchinnikov, and Steinegger
399 2021) running three iterations of the Alphafold2 algorithm (Jumper et al. 2021) trained
400 on the multimer dataset (Evans et al. 2021) on a local HPC equipped with NVIDIA
401 Ampere A100 80Go GPU cards. The five models converged toward similar
402 conformations and obtained high confidence and quality scores with pLDDTs in the
403 range [79.1, 85] and [72.6, 80.2] and pTMscore in the range [0.64, 0.662]. The model
404 with highest pTMscore was relaxed using rosetta relax protocols to remove steric

clashes constrained by the starting structure using the -relax:constrain_relax_to_start_coords option (Leman et al. 2020), and the model with the lowest rosetta global energy was used for structural analysis. Conservation analysis mapped at the structure of the model were performed using the ConSurf server (Ashkenazy et al. 2016).

Cytological techniques

Meiotic chromosome spreads on anthers were performed as previously described (Ross, Fransz, and Jones 1996). Chromosomes were stained with DAPI (1 µg/ml) Images were acquired and processed using a ZEISS microscope (AXIO-Imager.Z2) under a 100× oil immersion objective with ZEN software and figures were prepared using Adobe Photoshop.

Yeast two-hybrid and pull down

Clones were generated using the Gateway cloning system (Thermo Fisher Scientific); the desired inserts were cloned into pDONR221 as pENTR clones and then into different destination vectors using the LR clonase recombination method (Thermo Fisher Scientific). We generated full-length ORF pENTR clones for AtFANCC, AtFANCE, and AtMHF2 from an inflorescence cDNA library of Arabidopsis. One additional ORF pENTR of AtFANCC was cloned without a stop codon for in-frame C-terminal fusion and both ORF pENTR clones of AtFANCC were used for GSrhino-tagged pulldown. In yeast two-hybrid assays, we used two destination vectors, pGADT7-GW as bait and pGBKT7-GW as prey. The ORF pENTR clones of AtFANCC, AtFANCE, and AtMHF2 were cloned into both destination vectors by LR reaction. The ORF of AtFANCF was cloned into the pGBKT7 and PACT2 AD convectional vector using the NCO1, Sal1, and NCO1, XHO1 restriction enzymes, respectively. All pENTR

clones and final clones were verified thoroughly by Sanger sequencing to ensure mutation-free cloning and in-frame fusion. Plasmids of bait and prey clones were transformed into the haploid yeast strains AH109 and Y187, and then yeast two-hybrid assays were performed in a Gal4-based system from Clontech in a diploid strain by mating as previously described (Rossignol et al. 2007; Seguela-Arnaud et al. 2017).

Arabidopsis cell suspension cultures expressing N-terminal GSrhino-tagged FANCC and for C-terminal GSrhino-tagged FANCC were used for pull-down as previously described (Van Leene et al. 2019; Cromer et al. 2019). Co-purified proteins were identified using standard protocols utilizing on bead-digested sample evaluated on a Q Exactive mass spectrometer (Thermo Fisher Scientific) (Van Leene et al. 2015). After identification, the protein list was filtered for false-positives using a list of non-specific proteins, which was assembled as previously reported (Van Leene et al. 2015). Semi-quantitative analysis using the average normalized spectral abundance factors (NSAF) of the discovered proteins in the FANCC pull-downs was used to identify true interactors that may have been filtered out due to their classification in the list of nonspecific proteins. Chosen proteins were identified with at least two peptides in at least two experiments and showed high (at least 10-fold) and significant [log10(P value (t test)) enrichment relative to estimated average NSAF values from a large dataset of pull-downs with nonrelated bait proteins.

FTL analysis

To measure recombination, we used fluorescent transgenic lines (FTL) (420) generated in a Col background. The used lines harbor seed coat expressing GFP (Chr 3:256,516-GFP) and dsRed (Chr 3:5,361,637-dsRed2) fluorescent protein markers in cis (Ziolkowski et al. 2015; Melamed-Bessudo et al. 2005). We quantified the

fluorescence of the seeds using the Fiji image analysis software (Schindelin et al. 2012), which identifies seeds and quantifies fluorescence intensity for each seed in all pictures. The output was analyzed using a pipeline that was created to normalize the data, plot the frequency of objects with each fluorescent color, plot the fluorescence intensity, and quantify the number of seeds with only one fluorescent color, allowing selection of the number of recombinant seeds. For F2, recombination was measured using the formula below, as reported in (Ziolkowski et al. 2015).

$$cM = 100 * (1 - [1 - \frac{2(N_G + N_R)}{N_T}]^{1/2}$$

For male and female backcrosses, recombination was measured as

$$cM = 100 * \frac{(N_G + N_R)}{N_T}$$

Where N_G is the number of green-only fluorescent seeds, N_R is the number of red-only fluorescent seeds and N_T is the total number of seeds counted.

We generated a segregating population (F2) from which we selected plants heterozygous for the markers in cis with the desired mutants and wild-type control. For each genotype, we used at least three biological replicates (independent plants) with at least three technical replicates, each of them containing a minimum of 400 seeds. To measure CO frequency independently in males and females, reciprocal crosses were made with wild-type Columbia (0). Differences between genotypes were tested by Chi2 on the proportion of recombined seeds (Ng+Nr) among total seeds.

Funding

This work was supported by core funding from the Max Planck Society (to R.M.), a Depart of Biotechnology Centre of Excellence grant (to I.S.), and the CEFIPRA project SMOKI (to R.M. and IS).

488 Acknowledgements

489 We thank Virginie Portemer for her help in *fancc-1* mapping. We thank Piotr A.
490 Ziolkowski for kindly providing the 420 FTL line. We thank the VIB proteomics core
491 facility for performing the Q Exactive analysis of the pull down samplesand Neysan
492 Donnelly for proofreading the manuscript.

493

494 Altschul, S. F., T. L. Madden, A. A. Schaffer, J. Zhang, Z. Zhang, W. Miller, and D. J. Lipman.
495 1997. 'Gapped BLAST and PSI-BLAST: a new generation of protein database search
496 programs', *Nucleic Acids Res*, 25: 3389-402.
497 Ashkenazy, H., S. Abadi, E. Martz, O. Chay, I. Mayrose, T. Pupko, and N. Ben-Tal. 2016.
498 'ConSurf 2016: an improved methodology to estimate and visualize evolutionary
499 conservation in macromolecules', *Nucleic Acids Res*, 44: W344-50.
500 Berchowitz, L. E., K. E. Francis, A. L. Bey, and G. P. Copenhaver. 2007. 'The role of
501 AtMUS81 in interference-insensitive crossovers in A. thaliana', *PLoS Genet*, 3: e132.
502 Borner, G. V., N. Kleckner, and N. Hunter. 2004. 'Crossover/noncrossover differentiation,
503 synaptonemal complex formation, and regulatory surveillance at the
504 leptotene/zygotene transition of meiosis', *Cell*, 117: 29-45.
505 Cheng, C. Y., V. Krishnakumar, A. P. Chan, F. Thibaud-Nissen, S. Schobel, and C. D. Town.
506 2017. 'Araport11: a complete reannotation of the Arabidopsis thaliana reference
507 genome', *Plant J*, 89: 789-804.
508 Crismani, W., C. Girard, N. Froger, M. Pradillo, J. L. Santos, L. Chelysheva, G. P.
509 Copenhaver, C. Horlow, and R. Mercier. 2012. 'FANCM limits meiotic crossovers',
510 *Science*, 336: 1588-90.
511 Cromer, L., S. Jolivet, D. K. Singh, F. Berthier, N. De Winne, G. De Jaeger, S. Komaki, M. A.
512 Prusicki, A. Schnittger, R. Guerois, and R. Mercier. 2019. 'Patronus is the elusive
513 plant securin, preventing chromosome separation by antagonizing separase', *Proc
514 Natl Acad Sci U S A*, 116: 16018-27.

de los Santos, T., N. Hunter, C. Lee, B. Larkin, J. Loidl, and N. M. Hollingsworth. 2003. 'The Mus81/Mms4 endonuclease acts independently of double-Holliday junction resolution to promote a distinct subset of crossovers during meiosis in budding yeast', *Genetics*, 164: 81-94.

Deakyne, J. S., and A. V. Mazin. 2011. 'Fanconi anemia: at the crossroads of DNA repair', *Biochemistry (Mosc)*, 76: 36-48.

Deans, A. J., and S. C. West. 2009. 'FANCM connects the genome instability disorders Bloom's Syndrome and Fanconi Anemia', *Mol Cell*, 36: 943-53.

———. 2011. 'DNA interstrand crosslink repair and cancer', *Nat Rev Cancer*, 11: 467-80.

Dereeper, A., V. Guignon, G. Blanc, S. Audic, S. Buffet, F. Chevenet, J. F. Dufayard, S. Guindon, V. Lefort, M. Lescot, J. M. Claverie, and O. Gascuel. 2008. 'Phylogeny.fr: robust phylogenetic analysis for the non-specialist', *Nucleic Acids Res*, 36: W465-9.

Dorn, A., L. Feller, D. Castri, S. Rohrig, J. Enderle, N. J. Herrmann, A. Block-Schmidt, O. Trapp, L. Kohler, and H. Puchta. 2019. 'An Arabidopsis FANCJ helicase homologue is required for DNA crosslink repair and rDNA repeat stability', *PLoS Genet*, 15: e1008174.

Evans, Richard, Michael O'Neill, Alexander Pritzel, Natasha Antropova, Andrew Senior, Tim Green, Augustin Žídek, Russ Bates, Sam Blackwell, Jason Yim, Olaf Ronneberger, Sebastian Bodenstein, Michal Zielinski, Alex Bridgland, Anna Potapenko, Andrew Cowie, Kathryn Tunyasuvunakool, Rishub Jain, Ellen Clancy, Pushmeet Kohli, John Jumper, and Demis Hassabis. 2021. "Protein complex prediction with AlphaFold-Multimer." In.: Cold Spring Harbor Laboratory.

Fernandes, J. B., M. Duhamel, M. Seguela-Arnaud, N. Froger, C. Girard, S. Choinard, V. Solier, N. De Winne, G. De Jaeger, K. Gevaert, P. Andrey, M. Grelon, R. Guerois, R. Kumar, and R. Mercier. 2018. 'FIGL1 and its novel partner FLIP form a conserved complex that regulates homologous recombination', *PLoS Genet*, 14: e1007317.

Fernandes, J. B., M. Seguela-Arnaud, C. Larcheveque, A. H. Lloyd, and R. Mercier. 2018. 'Unleashing meiotic crossovers in hybrid plants', *Proc Natl Acad Sci U S A*, 115: 2431-36.

Fiesco-Roa, M. O., N. Giri, L. J. McReynolds, A. F. Best, and B. P. Alter. 2019. 'Genotype-phenotype associations in Fanconi anemia: A literature review', *Blood Rev*, 37: 100589.

Girard, C., L. Chelysheva, S. Choinard, N. Froger, N. Macaisne, A. Lemhemdi, J. Mazel, W. Crismani, and R. Mercier. 2015. 'AAA-ATPase FIDGETIN-LIKE 1 and Helicase FANCM Antagonize Meiotic Crossovers by Distinct Mechanisms', *PLoS Genet*, 11: e1005369.

Girard, C., W. Crismani, N. Froger, J. Mazel, A. Lemhemdi, C. Horlow, and R. Mercier. 2014. 'FANCM-associated proteins MHF1 and MHF2, but not the other Fanconi anemia factors, limit meiotic crossovers', *Nucleic Acids Res*, 42: 9087-95.

Higgins, J. D., J. Vignard, R. Mercier, A. G. Pugh, F. C. Franklin, and G. H. Jones. 2008. 'AtMSH5 partners AtMSH4 in the class I meiotic crossover pathway in Arabidopsis thaliana, but is not required for synapsis', *Plant J*, 55: 28-39.

Howlett, N. G., T. Taniguchi, S. Olson, B. Cox, Q. Waisfisz, C. De Die-Smulders, N. Persky, M. Grompe, H. Joenje, G. Pals, H. Ikeda, E. A. Fox, and A. D. D'Andrea. 2002. 'Biallelic inactivation of BRCA2 in Fanconi anemia', *Science*, 297: 606-9.

Huang, Y., J. W. Leung, M. Lowery, N. Matsushita, Y. Wang, X. Shen, D. Huong, M. Takata, J. Chen, and L. Li. 2014. 'Modularized functions of the Fanconi anemia core complex', *Cell Rep*, 7: 1849-57.

Ito, S., and T. Nishino. 2021. 'Structural analysis of the chicken FANCM-MHF complex and its stability', *Acta Crystallogr F Struct Biol Commun*, 77: 1-7.

Jumper, J., R. Evans, A. Pritzel, T. Green, M. Figurnov, O. Ronneberger, K. Tunyasuvunakool, R. Bates, A. Zidek, A. Potapenko, A. Bridgland, C. Meyer, S. A. A. Kohl, A. J. Ballard, A. Cowie, B. Romera-Paredes, S. Nikolov, R. Jain, J. Adler, T. Back, S. Petersen, D. Reiman, E. Clancy, M. Zielinski, M. Steinegger, M. Pacholska,

T. Berghammer, S. Bodenstein, D. Silver, O. Vinyals, A. W. Senior, K. Kavukcuoglu, P. Kohli, and D. Hassabis. 2021. 'Highly accurate protein structure prediction with AlphaFold', *Nature*, 596: 583-89.

Katoh, K., and D. M. Standley. 2013. 'MAFFT multiple sequence alignment software version 7: improvements in performance and usability', *Mol Biol Evol*, 30: 772-80.

Kolinjivadi, A. M., W. Crismani, and J. Ngeow. 2020. 'Emerging functions of Fanconi anemia genes in replication fork protection pathways', *Hum Mol Genet*, 29: R158-R64.

Kottemann, M. C., and A. Smogorzewska. 2013. 'Fanconi anaemia and the repair of Watson and Crick DNA crosslinks', *Nature*, 493: 356-63.

Kumar, R., M. Duhamel, E. Coutant, E. Ben-Nahia, and R. Mercier. 2019. 'Antagonism between BRCA2 and FIGL1 regulates homologous recombination', *Nucleic Acids Res*, 47: 5170-80.

Kurzbauer, M. T., M. Pradillo, C. Kerzendorfer, J. Sims, R. Ladurner, C. Oliver, M. P. Janisiw, M. Mosiolek, D. Schweizer, G. P. Copenhaver, and P. Schlogelhofer. 2018. 'Arabidopsis thaliana FANCD2 Promotes Meiotic Crossover Formation', *Plant Cell*, 30: 415-28.

Leman, J. K., B. D. Weitzner, S. M. Lewis, J. Adolf-Bryfogle, N. Alam, R. F. Alford, M. Aprahamian, D. Baker, K. A. Barlow, P. Barth, B. Basanta, B. J. Bender, K. Blacklock, J. Bonet, S. E. Boyken, P. Bradley, C. Bystroff, P. Conway, S. Cooper, B. E. Correia, B. Coventry, R. Das, R. M. De Jong, F. DiMaio, L. Dsilva, R. Dunbrack, A. S. Ford, B. Frenz, D. Y. Fu, C. Geniesse, L. Goldschmidt, R. Gowthaman, J. J. Gray, D. Gront, S. Guffy, S. Horowitz, P. S. Huang, T. Huber, T. M. Jacobs, J. R. Jeliazkov, D. K. Johnson, K. Kappel, J. Karanicolas, H. Khakzad, K. R. Khar, S. D. Khare, F. Khatib, A. Khramushin, I. C. King, R. Kleffner, B. Koepnick, T. Kortemme, G. Kuenze, B. Kuhlman, D. Kuroda, J. W. Labonte, J. K. Lai, G. Lapidoth, A. Leaver-Fay, S. Lindert, T. Linsky, N. London, J. H. Lubin, S. Lyskov, J. Maguire, L. Malmstrom, E. Marcos, O. Marcu, N. A. Marze, J. Meiler, R. Moretti, V. K. Mulligan, S. Nerli, C. Norn, S. O'Conchuir, N. Ollikainen, S. Ovchinnikov, M. S. Pacella, X. Pan, H. Park, R. E.

597 Pavlovicz, M. Pethe, B. G. Pierce, K. B. Pilla, B. Raveh, P. D. Renfrew, S. S. R.
598 Burman, A. Rubenstein, M. F. Sauer, A. Scheck, W. Schief, O. Schueler-Furman, Y.
599 Sedan, A. M. Sevy, N. G. Sgourakis, L. Shi, J. B. Siegel, D. A. Silva, S. Smith, Y.
600 Song, A. Stein, M. Szegedy, F. D. Teets, S. B. Thyme, R. Y. Wang, A. Watkins, L.
601 Zimmerman, and R. Bonneau. 2020. 'Macromolecular modeling and design in
602 Rosetta: recent methods and frameworks', *Nat Methods*, 17: 665-80.
603 Letunic, I., and P. Bork. 2021. 'Interactive Tree Of Life (iTOL) v5: an online tool for
604 phylogenetic tree display and annotation', *Nucleic Acids Res*, 49: W293-W96.
605 Leveille, F., E. Blom, A. L. Medhurst, P. Bier, H. Laghmani el, M. Johnson, M. A. Rooimans,
606 A. Sobeck, Q. Waisfisz, F. Arwert, K. J. Patel, M. E. Hoatlin, H. Joenje, and J. P. de
607 Winter. 2004. 'The Fanconi anemia gene product FANCF is a flexible adaptor protein',
608 *J Biol Chem*, 279: 39421-30.
609 Lopez-Martinez, D., M. Kupculak, D. Yang, Y. Yoshikawa, C. C. Liang, R. Wu, S. P. Gygi,
610 and M. A. Cohn. 2019. 'Phosphorylation of FANCD2 Inhibits the FANCD2/FANCI
611 Complex and Suppresses the Fanconi Anemia Pathway in the Absence of DNA
612 Damage', *Cell Rep*, 27: 2990-3005 e5.
613 Lossaint, G., M. Larroque, C. Ribeyre, N. Bec, C. Larroque, C. Decaillet, K. Gari, and A.
614 Constantinou. 2013. 'FANCD2 binds MCM proteins and controls replisome function
615 upon activation of s phase checkpoint signaling', *Mol Cell*, 51: 678-90.
616 Melamed-Bessudo, C., E. Yehuda, A. R. Stuitje, and A. A. Levy. 2005. 'A new seed-based
617 assay for meiotic recombination in Arabidopsis thaliana', *Plant J*, 43: 458-66.
618 Mirdita, M., L. von den Driesch, C. Galiez, M. J. Martin, J. Soding, and M. Steinegger. 2017.
619 'Uniclust databases of clustered and deeply annotated protein sequences and
620 alignments', *Nucleic Acids Res*, 45: D170-D76.
621 Mirdita, Milot, Sergey Ovchinnikov, and Martin Steinegger. 2021. 'ColabFold - Making protein
622 folding accessible to all', *bioRxiv*: 2021.08.15.456425.
623 Niraj, J., A. Farkkila, and A. D. D'Andrea. 2019. 'The Fanconi Anemia Pathway in Cancer',
624 *Annu Rev Cancer Biol*, 3: 457-78.

625 Polito, D., S. Cukras, X. Wang, P. Spence, L. Moreau, A. D. D'Andrea, and Y. Kee. 2014.
626 'The carboxyl terminus of FANCE recruits FANCD2 to the Fanconi Anemia (FA) E3
627 ligase complex to promote the FA DNA repair pathway', *J Biol Chem*, 289: 7003-10.
628 Pyatnitskaya, A., V. Borde, and A. De Muyt. 2019. 'Crossing and zipping: molecular duties of
629 the ZMM proteins in meiosis', *Chromosoma*, 128: 181-98.
630 Rajendra, E., V. H. Oestergaard, F. Langevin, M. Wang, G. L. Dornan, K. J. Patel, and L. A.
631 Passmore. 2014. 'The genetic and biochemical basis of FANCD2 monoubiquitination',
632 *Mol Cell*, 54: 858-69.
633 Rosenberg, P. S., M. H. Greene, and B. P. Alter. 2003. 'Cancer incidence in persons with
634 Fanconi anemia', *Blood*, 101: 822-6.
635 Ross, K. J., P. Fransz, and G. H. Jones. 1996. 'A light microscopic atlas of meiosis in
636 Arabidopsis thaliana', *Chromosome Res*, 4: 507-16.
637 Rossignol, P., S. Collier, M. Bush, P. Shaw, and J. H. Doonan. 2007. 'Arabidopsis POT1A
638 interacts with TERT-V(I8), an N-terminal splicing variant of telomerase', *J Cell Sci*,
639 120: 3678-87.
640 Sawyer, S. L., L. Tian, M. Kahkonen, J. Schwartzentruber, M. Kircher, Genomics University
641 of Washington Centre for Mendelian, Forge Canada Consortium, J. Majewski, D. A.
642 Dyment, A. M. Innes, K. M. Boycott, L. A. Moreau, J. S. Moilanen, and R. A.
643 Greenberg. 2015. 'Biallelic mutations in BRCA1 cause a new Fanconi anemia
644 subtype', *Cancer Discov*, 5: 135-42.
645 Schindelin, J., I. Arganda-Carreras, E. Frise, V. Kaynig, M. Longair, T. Pietzsch, S. Preibisch,
646 C. Rueden, S. Saalfeld, B. Schmid, J. Y. Tinevez, D. J. White, V. Hartenstein, K.
647 Eliceiri, P. Tomancak, and A. Cardona. 2012. 'Fiji: an open-source platform for
648 biological-image analysis', *Nat Methods*, 9: 676-82.
649 Schneeberger, K., S. Ossowski, F. Ott, J. D. Klein, X. Wang, C. Lanz, L. M. Smith, J. Cao, J.
650 Fitz, N. Warthmann, S. R. Henz, D. H. Huson, and D. Weigel. 2011. 'Reference-
651 guided assembly of four diverse Arabidopsis thaliana genomes', *Proc Natl Acad Sci U*
652 *S A*, 108: 10249-54.

653 Seguela-Arnaud, M., S. Choinard, C. Larcheveque, C. Girard, N. Froger, W. Crismani, and
654 R. Mercier. 2017. 'RMI1 and TOP3alpha limit meiotic CO formation through their C-
655 terminal domains', *Nucleic Acids Res*, 45: 1860-71.
656 Shakeel, S., E. Rajendra, P. Alcon, F. O'Reilly, D. S. Chorev, S. Maslen, G. Degliesposti, C.
657 J. Russo, S. He, C. H. Hill, J. M. Skehel, S. H. W. Scheres, K. J. Patel, J. Rappsilber,
658 C. V. Robinson, and L. A. Passmore. 2019. 'Structure of the Fanconi anaemia
659 monoubiquitin ligase complex', *Nature*, 575: 234-37.
660 Shimamura, A., and B. P. Alter. 2010. 'Pathophysiology and management of inherited bone
661 marrow failure syndromes', *Blood Rev*, 24: 101-22.
662 Singh, T. R., D. Saro, A. M. Ali, X. F. Zheng, C. H. Du, M. W. Killen, A. Sachpatzidis, K.
663 Wahengbam, A. J. Pierce, Y. Xiong, P. Sung, and A. R. Meetei. 2010. 'MHF1-MHF2,
664 a histone-fold-containing protein complex, participates in the Fanconi anemia
665 pathway via FANCM', *Mol Cell*, 37: 879-86.
666 Smogorzewska, A., S. Matsuoka, P. Vinciguerra, E. R. McDonald, 3rd, K. E. Hurov, J. Luo,
667 B. A. Ballif, S. P. Gygi, K. Hofmann, A. D. D'Andrea, and S. J. Elledge. 2007.
668 'Identification of the FANCI protein, a monoubiquitinated FANCD2 paralog required
669 for DNA repair', *Cell*, 129: 289-301.
670 Soding, J. 2005. 'Protein homology detection by HMM-HMM comparison', *Bioinformatics*, 21:
671 951-60.
672 Stanley, E. C., P. A. Azzinaro, D. A. Vierra, N. G. Howlett, and S. Q. Irvine. 2016. 'The
673 Simple Chordate Ciona intestinalis Has a Reduced Complement of Genes Associated
674 with Fanconi Anemia', *Evol Bioinform Online*, 12: 133-48.
675 Steinegger, M., and J. Soding. 2017. 'MMseqs2 enables sensitive protein sequence
676 searching for the analysis of massive data sets', *Nat Biotechnol*, 35: 1026-28.
677 Swuec, P., L. Renault, A. Borg, F. Shah, V. J. Murphy, S. van Twest, A. P. Snijders, A. J.
678 Deans, and A. Costa. 2017. 'The FA Core Complex Contains a Homo-dimeric
679 Catalytic Module for the Symmetric Mono-ubiquitination of FANCI-FANCD2', *Cell*
680 *Rep*, 18: 611-23.

Tao, Y., C. Jin, X. Li, S. Qi, L. Chu, L. Niu, X. Yao, and M. Teng. 2012. 'The structure of the FANCM-MHF complex reveals physical features for functional assembly', *Nat Commun*, 3: 782.

Van Leene, J., D. Eeckhout, B. Cannoot, N. De Winne, G. Persiau, E. Van De Slijke, L. Vercruysse, M. Dedecker, A. Verkest, K. Vandepoele, L. Martens, E. Witters, K. Gevaert, and G. De Jaeger. 2015. 'An improved toolbox to unravel the plant cellular machinery by tandem affinity purification of Arabidopsis protein complexes', *Nat Protoc*, 10: 169-87.

Van Leene, J., C. Han, A. Gadeyne, D. Eeckhout, C. Matthijs, B. Cannoot, N. De Winne, G. Persiau, E. Van De Slijke, B. Van de Cotte, E. Stes, M. Van Bel, V. Storme, F. Impens, K. Gevaert, K. Vandepoele, I. De Smet, and G. De Jaeger. 2019. 'Capturing the phosphorylation and protein interaction landscape of the plant TOR kinase', *Nat Plants*, 5: 316-27.

Walden, H., and A. J. Deans. 2014. 'The Fanconi anemia DNA repair pathway: structural and functional insights into a complex disorder', *Annu Rev Biophys*, 43: 257-78.

Wang, S., R. Wang, C. Peralta, A. Yaseen, and N. P. Pavletich. 2021. 'Structure of the FA core ubiquitin ligase closing the ID clamp on DNA', *Nat Struct Mol Biol*, 28: 300-09.

Waterhouse, A. M., J. B. Procter, D. M. Martin, M. Clamp, and G. J. Barton. 2009. 'Jalview Version 2--a multiple sequence alignment editor and analysis workbench', *Bioinformatics*, 25: 1189-91.

Yan, Z., M. Delannoy, C. Ling, D. Daee, F. Osman, P. A. Muniandy, X. Shen, A. B. Oostra, H. Du, J. Steltenpool, T. Lin, B. Schuster, C. Decaillet, A. Stasiak, A. Z. Stasiak, S. Stone, M. E. Hoatlin, D. Schindler, C. L. Woodcock, H. Joenje, R. Sen, J. P. de Winter, L. Li, M. M. Seidman, M. C. Whitby, K. Myung, A. Constantinou, and W. Wang. 2010. 'A histone-fold complex and FANCM form a conserved DNA-remodeling complex to maintain genome stability', *Mol Cell*, 37: 865-78.

Youds, J. L., and S. J. Boulton. 2011. 'The choice in meiosis - defining the factors that influence crossover or non-crossover formation', *J Cell Sci*, 124: 501-13.

Zapata, L., J. Ding, E. M. Willing, B. Hartwig, D. Bezdan, W. B. Jiao, V. Patel, G. Velikkakam James, M. Koornneef, S. Ossowski, and K. Schneeberger. 2016. 'Chromosome-level assembly of Arabidopsis thaliana Ler reveals the extent of translocation and inversion polymorphisms', *Proc Natl Acad Sci U S A*, 113: E4052-60.

Zhang, X. Y., J. Langenick, D. Traynor, M. M. Babu, R. R. Kay, and K. J. Patel. 2009. 'Xpf and not the Fanconi anaemia proteins or Rev3 accounts for the extreme resistance to cisplatin in Dictyostelium discoideum', PLoS Genet, 5: e1000645.

Zimmermann, L., A. Stephens, S. Z. Nam, D. Rau, J. Kubler, M. Lozajic, F. Gabler, J. Soding, A. N. Lupas, and V. Alva. 2018. 'A Completely Reimplemented MPI Bioinformatics Toolkit with a New HHpred Server at its Core', *J Mol Biol*, 430: 2237-43.

Ziolkowski, P. A., L. E. Berchowitz, C. Lambing, N. E. Yelina, X. Zhao, K. A. Kelly, K. Choi, L. Ziolkowska, V. June, E. Sanchez-Moran, C. Franklin, G. P. Copenhaver, and I. R. Henderson. 2015. 'Juxtaposition of heterozygous and homozygous regions causes reciprocal crossover remodelling via interference during Arabidopsis meiosis', *Elife*, 4.

Figure 1. Analysis of fertility of *zmm* suppressor mutants.

(A) Each dot indicates the fertility of an individual plant, measured as the number of seeds per fruit averaged on ten fruits. The mean fertility for each genotype is shown by a red bar. Each mutant was compared to sibling controls grown together, and the data of independent experiments are shown in Figure S2. Some genotypes were represented in several experiments and their data were pooled for this figure. Stars summarize the one-way ANOVA followed by Sidak test shown in Figure S2. (B–E)

734 Representative fruits of *wild type, fancc-2, msh4*, and *fancc-2 msh4*, cleared with 70%
735 ethanol.

736

737 **Figure 2. Structural analysis of the experimental human and modeled *A. thaliana***
738 **FANCC-FANCE-FANCF complexes.**

739 (A) Structural representation of the human FANC core complex (PDB:7KZP) (Wang et
740 al. 2021) Most of the subunits are shown in gray with the exception of those in direct
741 contact with the human FANCC (light green), namely hFANCE (light pink), hFANCL
742 (yellow) and hFANCF (light blue). A zoomed-in view of the four subunits is shown in
743 the inset on the right with the contact region between hFANCL and hFANCC
744 highlighted by a dotted rectangle. (B) AlphaFold2 structural model of the AtFANCC-
745 AtFANCE-AtFANCF complex represented as a cartoon in two orientations with a
746 dotted square indicating the C-terminal domain of FANCE located in a region of
747 FANCC that directly binds to the FANCL subunit in the human FANC core complex
748 structure. (C) Same view as (B) with AtFANCC shown as a surface and colored
749 according to conservation from white to red for the least to most conserved positions.
750 Pymol software was used to draw the different structures (The PyMOL Molecular
751 Graphics System, Version 2.0 Schrödinger, LLC).

752

753

754 **Figure 3. Metaphase chromosome spreads of male meiocytes.**

755 (A) Wild type with five bivalents, (*B*) *msh4* with one bivalent, (C) *fancc-2* with four
756 bivalents and one pair of univalents. (D) *fancc-2* with five bivalents (*E*) *fancc-2 msh4*
757 with two bivalents (F) *fancc-2 fance fancf msh4* with two bivalents. Scale bar, 10 μm.

(G) Quantification of bivalents at metaphase I. The proportion of cells with 0–5 bivalents is shown with a color code. The number of analyzed cells and the average bivalent number per cell is shown for each genotype. All the genotypes are in the Col background, except when Ler is mentioned.

Figure 4. Recombination in *fancc*, *fance* and *fancf* mutant.

(A) Recombination was measured in seeds produced by crosses with wild type (female and male) or after selfing. Each dot represents the recombination frequency measured in an individual plant, and the red lines show the mean. *P* values are from two-sided Fisher's exact test on the proportion of recombined seeds. Raw data are shown in Table S2 (B–D). Representative image of seeds from a 420/++ hemizygote imaged under bright-field, red fluorescence channel, green fluorescence channel, and merged fluorescence.

Figure 5. Combining *fanc and mus81* mutations leads to reduced fertility and chromosome fragmentation at meiosis. (A) Each dot indicates the fertility of an individual plant, measured as the number of seeds per fruit averaged on ten fruits. The means for each genotype are shown by red bars. Each double mutant was compared to sibling controls grown together; the independent experiments are shown in Figure S8. Wild type and *mus81* control were represented in several experiments and their data are pooled in this plot. (B) Quantification of cells with and without chromosome fragments. N=number of cells analyzed for each genotype. Stars summarize the one-way ANOVA followed by Sidak test shown in Figure S8. (C–J) Chromosome spreads

781 of male meiocytes (Scale bar, 10 μm). Arrow heads indicate chromosome fragments.

782 (C, G) *mus81*. (D, H) *fancc-2 mus81.* (E, I) *fance mus81* (F, J) *fancf mus81.*

783

784

785

Table 1. Summary of the *zmm* suppressor screen results.

		Number of alleles identified in each screen					
		total	*zip4*	*hei10*	*msh5*	*shoc1*	*msh4 (Ler)*
	Number of M2 populations screened	**~7,000**	*~2,000*	*~2,000*	*~1,000*	*~1,000*	*~1,000*
identified gene	*FANCC*	**1**					1
	FANCM	**29**	5	5	4	8	7
	MHF2	**4**	1	2			1
	TOP3	**4**		3			1
	RECQ4	**3**					3
	RMI1	**2**				1	1
	FIGL1	**15**	2	5	3	3	2
	FLIP	**1**		1			
	total	**59**	8	16	7	12	16

A suppressor screen was performed in five *zmm* mutants (*zip4, hei10, msh5, shoc1, and msh4*). One to two thousand independent M2 populations were screened for each *zmm*. At total of 59 causal mutations falling in eight genes were identified and we report the number of alleles identified per gene and per screen. The colors represent three distinct pathways (FA blue, BTR green, FIGL1 red). Note that *msh4* is in the Ler background while others are in Col. As RECQ4 is duplicated in Col but not in Ler, it could be found only in the *msh4* screen. The list of mutant alleles is shown in Table S1.

798 **Table 2. Pull-down protein purification using At3G60310/FANCC as bait.**

Gene Id	Protein name	CGSrhino PD1	CGSrhino PD2	CGSrhino PD3
At3G60310	FANCC	19	18	15
AT4G29560	FANCE	6	4	5
AT5G65740	FANCL	5	4	4
At1G78790	MHF2	2	-	3
AT1G35530	FANCM*	2	-	-

799

800 Three replicates of pull-down purifications (IP1, IP2 and IP3) followed by mass
801 spectrometry were performed using FANCC as a bait. After filtering (see material and
802 methods), the number of specific peptides is reported for each identified protein. *Only
803 identified in one experiment. MS data are shown in table S4.

804 **Figure S1. Schematic representation of the *AtFANCC*, *AtFANCE* and *AtFANCF***
805 **genes.**

806 Gene orientations are indicated by horizontal arrows. A vertical red line indicates a
807 point mutation, and red triangles indicate T-DNA insertions. The numbers on inverted
808 triangles and vertical line denote corresponding alleles of *fancc*. Exons are indicated
809 by a solid black box, while introns and untranslated regions (UTR) are represented by
810 a line.

811

812 **Figure S2. Analysis of fertility of *zmm* suppreso*r* mutants**. Each dot indicates the
813 fertility of an individual plant, measured as the number of seeds per fruit averaged on
814 ten fruits. The mean for each genotype is represented by a red bar. The vertical lines
815 separate experiments performed independently. Within each experiment, all plants
816 were cultivated together in a population segregating for the mutations. *P* values are
817 from one-way ANOVA followed by the Sidak test for multiple comparisons.

818 **Figure S3. Superimposition of the five models of the AtFANCC-AtFANCE-**
819 **AtFANCF complex calculated by AlphaFold2.** (A) Representation showing the
820 convergence of the five models of FANCC and FANCF superimposed with only one
821 example of FANCE for the sake of clarity. (B) Same view as (A) with the five models
822 of FANCE shown in different shades of pink color. In the top panel, the C-terminal
823 orientation of FANCE is found to be poorly defined due to the flexible short linker
824 connecting it to its N-terminal domain (lower panel) whose orientation is, in contrast,
825 very well defined due to a large binding interface with FANCC. (C) 2D map of the
826 predicted alignment error (PAE) calculated by AlphaFold2 which can be used as a
827 proxy for the reliability of the structural model of every subunit and of the binding
828 interfaces. As in panel B, the interface between the N-terminal domain of FANCE and

829 FANCC is predicted to be accurately modeled, while its C-terminal domain is not
830 predicted to bind as specifically and reliably. (D) Representation of the PAE map
831 calculated for each of the five AlphaFold2 models.

832

833 **Figure S4. Multiple sequence alignment of FANCC orthologs in ten**
834 **representative plant species.** The structural model of the complex is shown on top.
835 The abbreviated species names and their NCBI indexes are provided in the headers.
836 The regions of FANCC interacting with FANCF and FANCE are indicated by blue and
837 pink straight lines around them, respectively. MSA is represented using JalView
838 (Waterhouse et al. 2009).

839

840 **Figure S5. Circular representation of the phylogenetic tree of FANCC orthologs.**
841 A phylogenetic tree comprising 72 plant species orthologs was calculated using PhyML
842 (Dereeper et al. 2008) and represented with iTOL(Letunic and Bork 2021). A sampled
843 multiple sequence alignment of nine FANCC orthologs in the species labelled at the
844 end of the branches is available in Figure S4. Confidence supports for each clade in
845 the tree are indicated by the size of the gray disks; the reliable branches are green,
846 while the unreliable ones range from yellow to red.

847

848 **Figure S6. FANCC interactions tested by yeast two-hybrid.**

849 Proteins of interest were fused with Gal4 DNA binding domain (BD) as bait and with
850 Gal4 activation domain as prey (AD), respectively, then expressed in yeast cells. For
851 each combination, yeast cells were spotted on non-selective medium (-LW) as control

and moderately selective media (-LWH). Growth on -LWH is interpreted as direct interaction between the two tested proteins.

Figure S7. Chromosome spreads of male meiocytes at metaphase I.

(A–B) *fance* (C–D) *fancf,*A and C are normal metaphase I with five bivalents while B and D have one pair of univalent and four bivalents. (Scale bar, 10 μm).

Figure S8. Analysis of fertility of *fanc* mutants combined with *mus81*. Each dot indicates the fertility of an individual plant, measured as the number of seeds per fruit averaged on ten fruits. The mean for each genotype is represented by a red bar. The vertical lines separate independent experiments. All plants were cultivated in parallel in each experiment, and the wild-type controls were mutant siblings except for the *mus81 fance* combination because the two genes are linked. In this latter case, *mus81* segregating and *fance* segregating population mutants were used as controls. *P* values are from one-way ANOVA followed by the Sidak test for multiple comparisons.

Figure S9. Combining *fanc* and *mus81* mutations instigates chromosome fragmentation at meiosis. (A–K) Chromosome spreads of male meiocytes (Scale bar, 10 μm). Arrow heads indicate chromosome fragments.

Table S1. Mutations identified in the *zmm* suppressor screen.

Table S2. FTL seed data used to measure genetic recombination.

Table S3. Primers used in this study.

Table S4. MS data

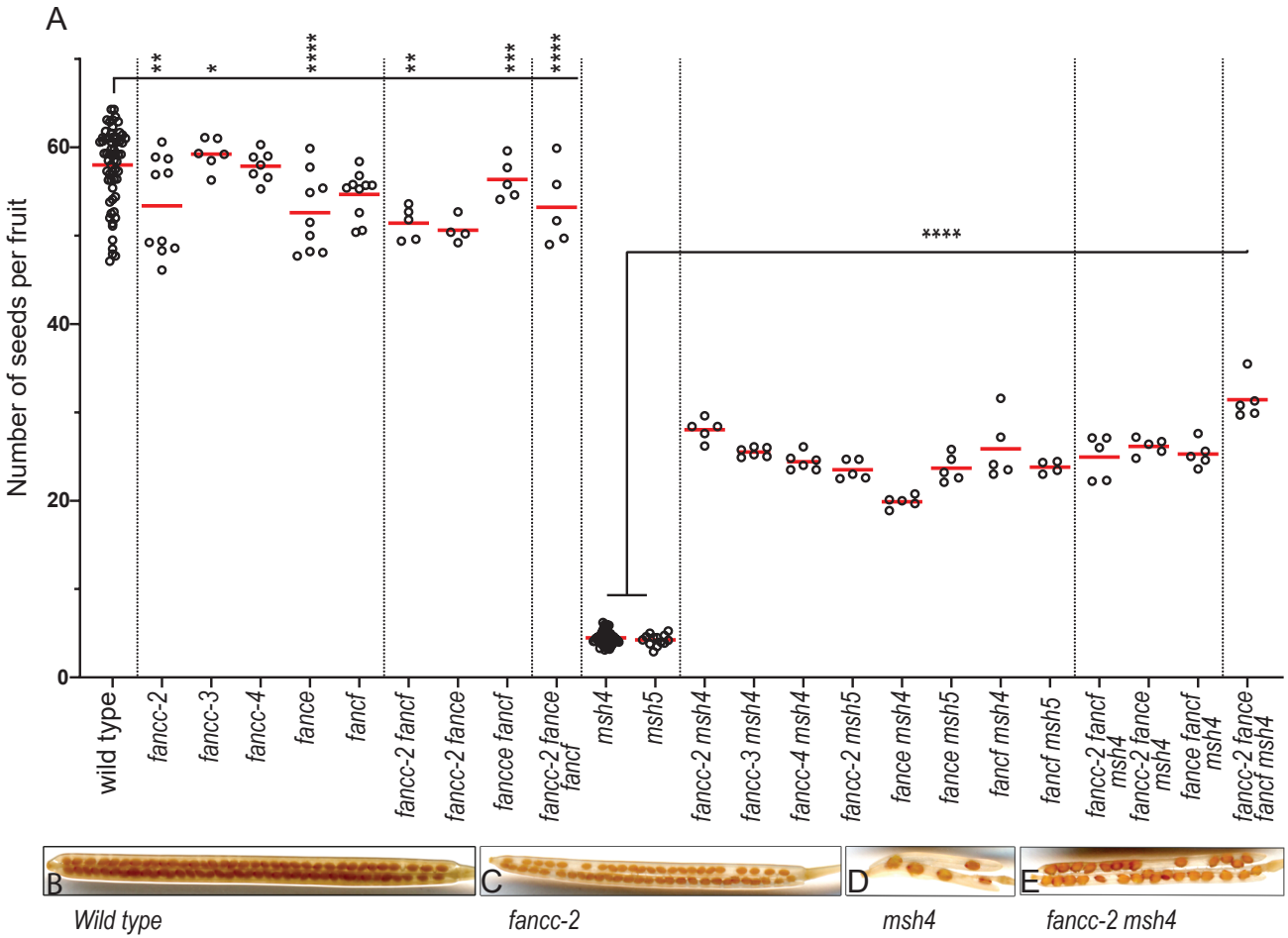

Figure 1. Analysis of fertility of zmm suppressor mutants.
(A) Each dot indicates the fertility of an individual plant, measured as the number of seeds per fruit averaged on ten fruits. The mean fertility for each genotype is shown by a red bar. Each mutant was compared to sibling controls grown together, and the data of independent experiments are shown in Figure S2. Some genotypes were represented in several experiments and their data were pooled for this figure. Stars summarize the one-way ANOVA followed by Sidak test shown in Figure S2. (B–E) Representative fruits of wild type, *fancc-2, msh4*, and *fancc-2 msh4*, cleared with 70% ethanol.

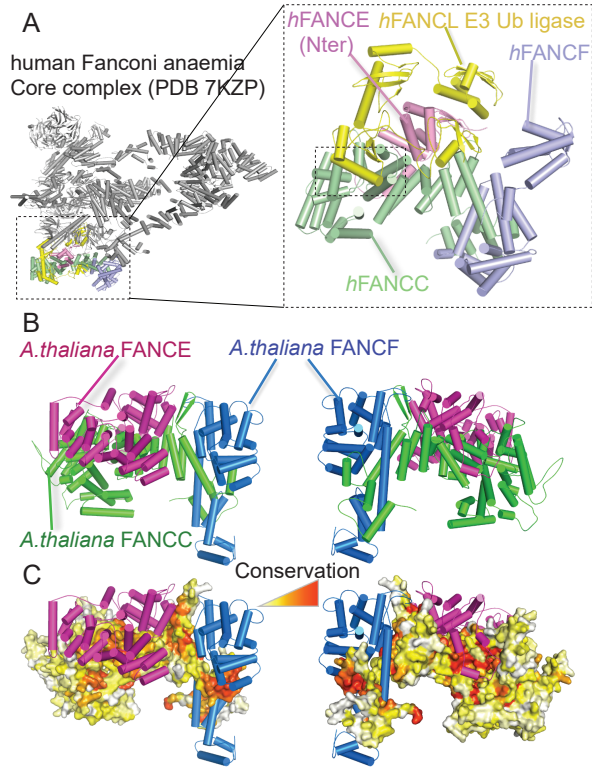

Figure 2. Structural analysis of the experimental human and modeled A. thaliana FANCC-FANCE-FANCF complexes.

(A) Structural representation of the human FANC core complex (PDB:7KZP) (Wang et al. 2021) Most of the subunits are shown in gray with the exception of those in direct contact with the human FANCC (light green), namely hFANCE (light pink), hFANCL (yellow) and hFANCF (light blue). A zoomed-in view of the four subunits is shown in the inset on the right with the contact region between hFANCL and hFANCC highlighted by a dotted rectangle. (B) AlphaFold2 structural model of the AtFANCC-AtFANCE-AtFANCF complex represented as a cartoon in two orientations with a dotted square indicating the C-terminal domain of FANCE located in a region of FANCC that directly binds to the FANCL subunit in the human FANC core complex structure. (C) Same view as (B) with AtFANCC shown as a surface and colored according to conservation from white to red for the least to most conserved positions. Pymol software was used to draw the different structures (The PyMOL Molecular Graphics System, Version 2.0 Schrödinger, LLC).

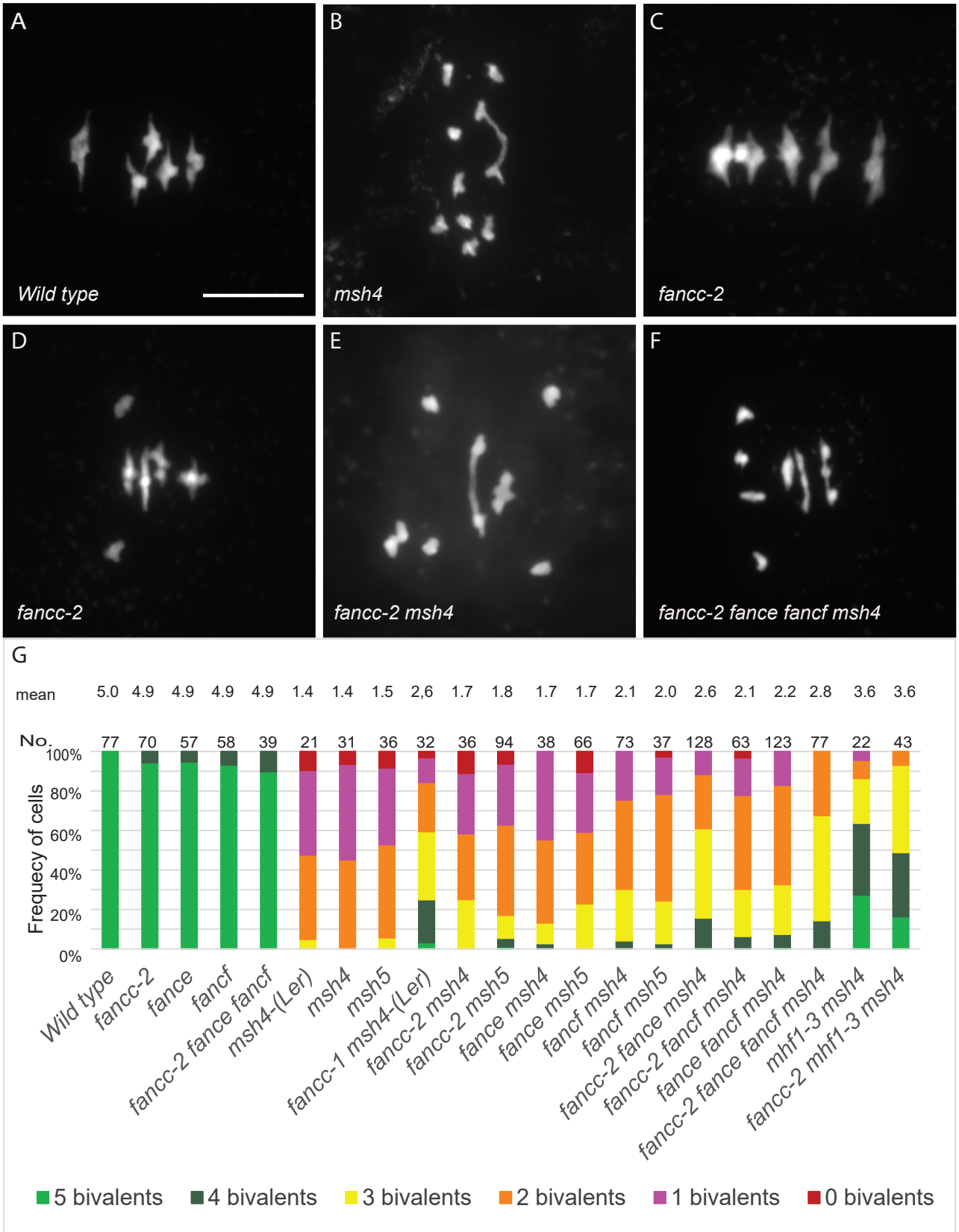

Figure 3. Metaphase chromosome spreads of male meiocytes.
(A) Wild type with five bivalents, (B) *msh4* with one bivalent, (C) *fancc-2* with four bivalents and one pair of univalents. (D) *fancc-2* with five bivalents (E) *fancc-2 msh4* with two bivalents (F) *fancc-2 fance fancf msh4* with two bivalents. Scale bar, 10 μm. (G) Quantification of bivalents at metaphase I. The proportion of cells with 0–5 bivalents is shown with a color code. The number of analyzed cells and the average bivalent number per cell is shown for each genotype. All the genotypes are in the Col background, except when Ler is mentioned.

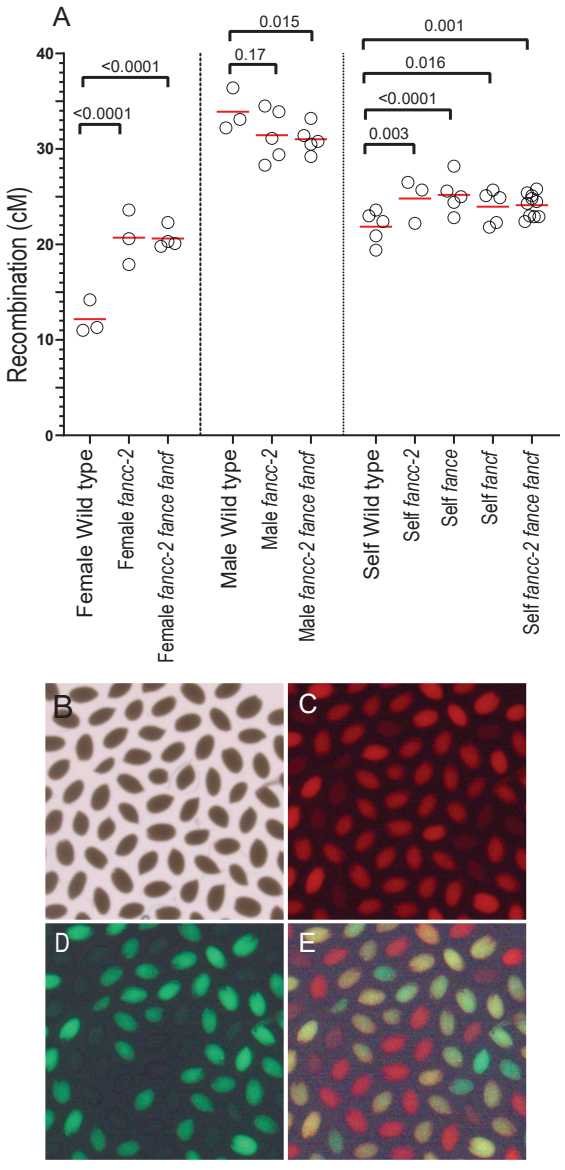

Figure 4. Recombination in fancc, fance and fancf mutant.
(A) Recombination was measured in seeds produced by crosses with wild type (female and male) or after selfing. Each dot represents the recombination frequency measured in an individual plant, and the red lines show the mean. P values are from two-sided Fisher's exact test on the proportion of recombined seeds. Raw data are shown in Table S2 (B–D). Representative image of seeds from a 420/++ hemizygote imaged under bright-field, red fluorescence channel, green fluorescence channel, and merged fluorescence.

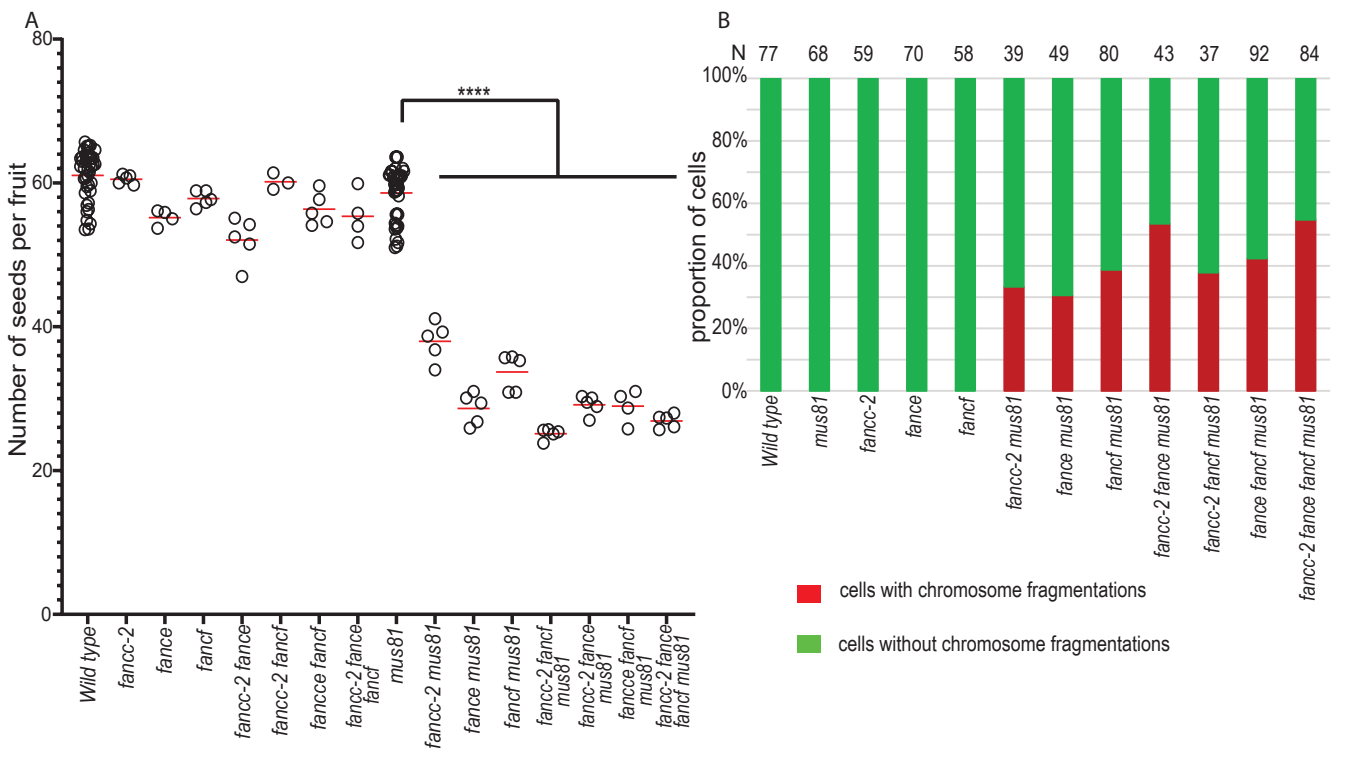

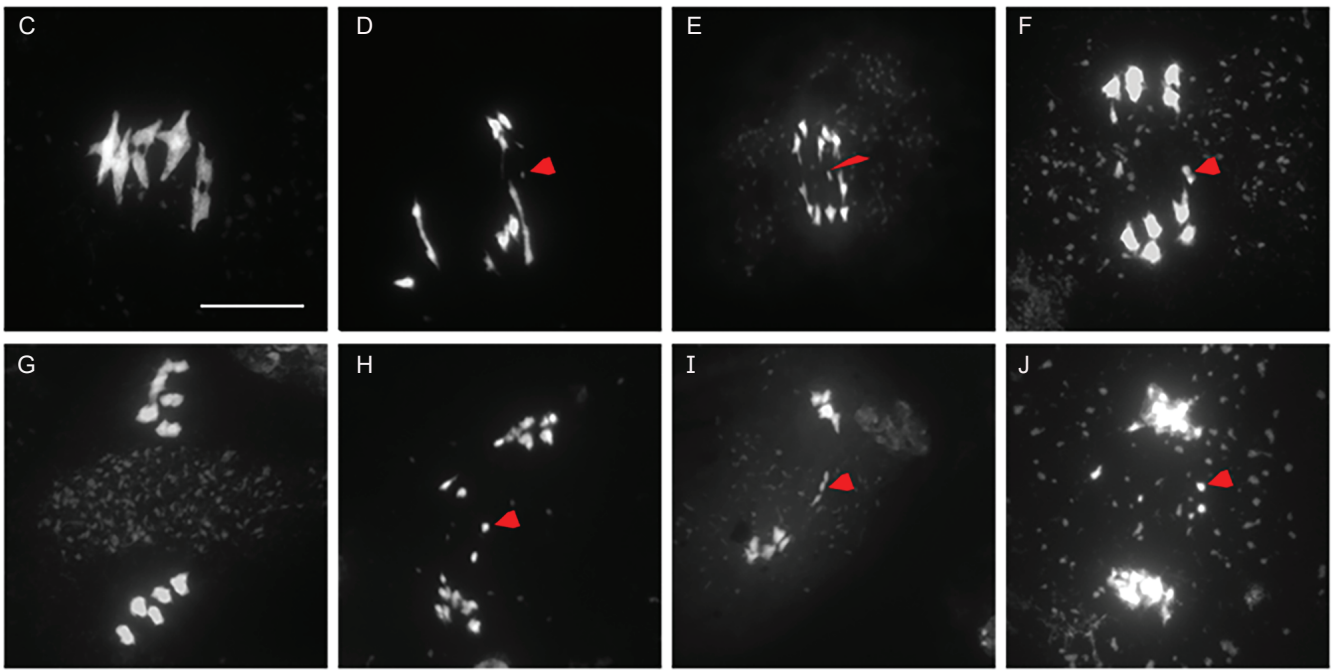

Figure 5. Combining fanc and mus81 mutations leads to reduced fertility and chromosome fragmentation at meiosis. (A) Each dot indicates the fertility of an individual plant, measured as the number of seeds per fruit averaged on ten fruits. The means for each genotype are shown by red bars. Each double mutant was compared to sibling controls grown together; the independent experiments are shown in Figure S8. Wild type and mus81 control were represented in several experiments and their data are pooled in this plot. (B) Quantification of cells with and without chromosome fragments. N=number of cells analyzed for each genotype. Stars summarize the one-way ANOVA followed by Sidak test shown in Figure S8. (C–J) Chromosome spreads of male meiocytes (Scale bar, 10 µm). Arrow heads indicate chromosome fragments. (C, G) mus81. (D, H) fancc-2 mus81. (E, I) fance mus81 (F, J) fancf mus81.